Int. J. Electrochem. Sci., 13 **(2018)** 10911 – 10933, doi: 10.20964/2018.11.82

International Journal of
ELECTROCHEMICAL
SCIENCE
www.electrochemsci.org

The Non-Adiabatic Model of Air-Breathing Micro Direct Methanol Fuel Cells

Luwen Wang, Yong Huang, Zhaoxia Yuan, Yumin Xu and Gaofeng Wang[*]

College of Electronic and Information Engineering, Hangzhou Dianzi University, *Hangzhou 310018*, China;
[*]E-mail: gaofeng@hdu.edu.cn

Received: 8 June 2018 / *Accepted:* 31 August 2018 / *Published:* 1 October 2018

A three-dimensional two-phase non-adiabatic model is proposed for air-breathing micro direct methanol fuel cells (DMFC). The coupled heat and mass transport, along with the electrochemical reactions occurring in the air-breathing DMFC are modeled. Based on this new non-adiabatic model, the reactants distribution and concentration distribution, the pressure and flow velocity distribution, the saturation distribution, the potential and current density distribution, the temperature distribution and their effects on the cell performance are carefully examined.

Keywords: air-breathing micro direct methanol fuel cells, model, three-dimensional two-phase

1. INTRODUCTION

With the popularization of mobile portable electronic products and the enhancement of their functions, higher performance is needed for the power supply system. Compared with other micro energy, fuel cell is a very promising energy, because it has the advantages of high energy conversion efficiency, more environment friendly, low temperature and rapid start-up, easy to integration and so on [1-3]. The fuel methanol in DMFC is not only low cost and easy to get and store, but also do not need reforming and purification. Moreover, low requirements of the operation condition are presented by DMFC. All merits mentioned above make DMFC more suitable for the future application of portable electronic products as an update power sources. However widespread application of the DMFC is also faced with many challenges, such as cathode water management, methanol crossover and anode gas management. In order to solve these problems in a better way, mathematical models plays an important role in the DMFC system, since it can provide a powerful and economical tool to analyze the complex transport processes, which are also hard to be studied experimentally.

According to the different fuel supply, DMFCs are divided into two types: passive and active.

Active DMFC requires additional devices such as fluid pump, blowers or fan to transmit reactants and products [4, 5]. These auxiliaries not only complicate the fuel cell system, but also reduce the energy density. On the other hand, the passive DMFC does not require auxiliary supplying devices, and provides the reactants and products on the basis of diffusion and natural convection. Although the performance of the passive DMFC is lower than the active one, it is still the best choice for portable power devices because of its simple structure, low weight, and limited parasitic power losses [6-11].

In order to comprehend the essentially coupled physicochemical processes occurring in DMFC, the experimentally interrelated parameters that affect the operation of the DMFC must be quantified. Numerical modeling is important to guide the experiments and optimize the parameters in DMFC. Most of the previous models were developed based on the 1D or 2D model [12-21]. However, the 1D or 2D model cannot reflect the all aspects of two-phase mass transfer processes occurring in the DMFC. Hence, in order to simulate the mass transfer process of DMFC, the development of the 3D two-phase mass transport model is necessary [22-26].

In recent years, several two-phase models for DMFCs have been published in the literature. Murgia [22] put forward a 1D model in view of phenomenological transport equations. Take into account of the interaction of the two-phase flow in the diffusion layer, this model introduced a Gaussian function to approximately calculate the effect of capillary pressure on the effective gas porosity. Chen [26] presented a 2D two-phase thermal model for passive DMFCs. In which the heat transfer effect had been developed based on the unsaturated flow theory in porous media. Their model simulated and studied the effects of different operating and design parameters of the current collectors on cell performance. Yang [25] developed a 3D two-phase mass transport model for DMFCs. This 3D mass transport model was formed by integrating five sub-models, each simulating a specific component of the DMFC. The effect of non-equilibrium evaporation/condensation at the gas-liquid interface was also considered in this model. Wang [24] proposed a two-dimensional (2D) non-isothermal model for passive DMFC in vertical operation. This model considered the effect of natural convection at the anode and coupled heat and mass transport of the whole cell with the electrochemical reactions occurring in the DMFC.

The purpose of this paper is to establish a 3D two-phase non-adiabatic model for air-breathing micro-DMFC, the main significance is more comprehensive consideration of actually environment and analysis of the influence of various parameters on the performance of the DMFC, so as to better optimize the performance of the DMFC. With this model, the distribution of the reactant concentration, the temperature, the potential and current density as well as the methanol crossover are studied and analyzed.

2. MATHEMATICAL MODEL

The calculation area of the 3D two-phase simulation model of the self-breathing DMFC is shown in Fig.1, which consists of an anode current collector(ACC), an anode diffusion layer(ADL), an anode catalyst layer(ACL), a proton exchange membrane(PEM), a cathode catalyst layer(CCL) and a cathode diffusion layer(CDL).

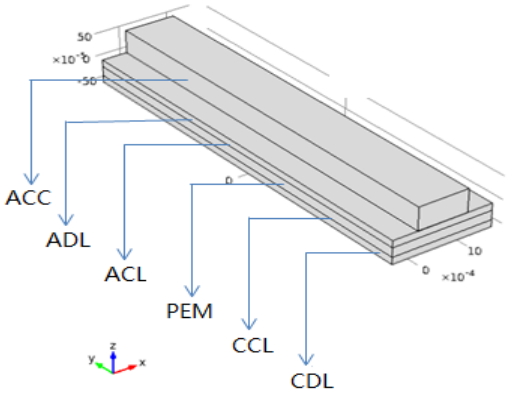

Figure 1. The computation domain of the model

In order to simplify the computations and processes, the mathematical model is formulated under the following assumptions and simplifications:

1. The DMFC is assumed to operate under steady-state conditions.
2. The heat and over-voltage generated by the electrochemical reaction and the Joule heat caused by current flowing through each component are ignored.
3. Because the thicknesses of ACL and CCL are much thinner than those of ADL, CDL and PEM, the catalytic layers are regarded as interfaces.
4. Methanol that penetrates into the cathode is assumed to be fully reacted.
5. The CO_2 gas that is dissolved in the liquid is negligible.
6. The cathode gas contains only nitrogen and oxygen, the carbon dioxide produced by oxidation of the methanol solution that permeates into the cathode is neglected.
7. The temperatures of the external walls of the cell are assumed to be constant according to the environmental conditions.

2.1. Two-phase mass transport in the ADL

At the anode of the cell, methanol is provided by the anode channel, transported through the diffusion layer to the catalytic layer, where some methanol permeates the cathode and is electrochemically oxidized to form carbon dioxide and electricity. The carbon dioxide produced by the reaction will be transported back through the diffusion layer to the channel and eventually exit the cell with the methanol solution stream. In the anode, the two-phase mass transport includes the anode flow field and the transmission of porous media is mainly related to the mass transfer of methanol, the production of emissions and electronic conservation. Several of the most important variables in the study were methanol concentration, liquid pressure, liquid saturation and gas fraction.

In the inner flow model of the channel, the incompressible flow N-S equation is used to express the momentum transfer of the methanol solution in the flow:

$$\rho \nabla \boldsymbol{u} = 0 \tag{1}$$

$$\rho_m \mu \nabla \mu = \nabla[-p + \eta(\nabla \mu + (\nabla \mu)^T)] + F \tag{2}$$

Where u is the velocity of solution, ρ is the density of the solution, μ is the dynamic viscosity

coefficient, *p* is liquid pressure and *F* is liquid phase pressure. *u* can be derived from Darcy's law.

$$\nabla(\rho u) = Q_m \tag{3}$$

$$\mu_l = \frac{-Kk_{rl}}{\mu_l}\nabla p_l \quad \mu_g = \frac{-Kk_{rg}}{\mu_g}\nabla p_g \tag{4}$$

Where *K*, k_{rl} and μ_l denoting the absolute permeability of the ADL, the relative permeability of the liquid phase and the viscosity of the liquid phase, respectively. The pressure difference between the gas phase and liquid phase is related to the capillary pressure:

$$p_c = p_g - p_l = \sigma\cos(\theta_c)(\frac{\varepsilon}{K})^{0.5}J(s) \tag{5}$$

Where *J*(s) represents the Leverette function, which is a function about liquid saturation in porous media:

$$J(s) = \begin{cases} 1.417(1-s) - 2.120(1-s)^2 + 1.263(1-s)^3 & 0 < \theta_c < 90^o \\ 1.417s - 2.120s^2 + 1.263s^3 & 90^o < \theta_c < 180^o \end{cases} \tag{6}$$

The mass transport in the porous medium of the anode is mainly convection and diffusion, which can be described as:

$$\nabla\cdot(-D_{eff}\nabla c) = R - u\nabla\cdot c \tag{7}$$

Where D_{eff} is the effective diffusivity of methanol in porous medium, *c* is the concentration of methanol solution, *R* is the reaction rate of methanol liquid.

2.2. Mass transport in the PEM

The membrane layer allows for the transfer of protons and insulates the electrons between ACL and CCL. Through the membrane, however the methanol solution also can penetrate from the anode to the cathode. Methanol permeates the membrane as the result of the concentration gradient and electro-osmotic drag by the proton transfer. Accordingly, the flux of methanol through the membrane, N_{cross} can be determined from:

$$N_{cross} = -D_{m,mem}^{eff}\frac{dC_{m,mem}}{dx} + n_d^m\frac{i}{F} \tag{9}$$

Where $-D_{m,mem}^{eff}$ is the effective diffusivity of methanol in the membrane, *F* is the Faraday's constant, n_d^m is the electro-osmotic drag coefficient of methanol, which can be determined from [27]:

$$n_d^m = n_d^w x_m \tag{10}$$

Where n_d^w is the electro-osmotic drag coefficient of water, x_m is the molar fraction of methanol.

2.3. Two-phase mass transport in the CDL

At the cathode of the cell, the oxygen is absorbed from the air and transferred to the CCL, react with electrons and protons to produce gaseous water. A portion of the oxygen reacts with the permeated methanol to produce liquid water and carbon dioxide, forming an internal current and a mixed potential. The liquid water is generated in the CCL and that permeated from the anode will

move outside of the cathode by the capillary force. Thus, this two-phase flow mass transport in the CDL can be modeled with the following equations:

$$-\nabla\cdot(-D_{O_2}^{eff}\nabla C_{O_2}^{cdl})=0 \quad \text{(gas phase)} \tag{11}$$

$$-\nabla\cdot(-D_{v}^{eff}\nabla C_{v}^{cdl})-R_w=0 \quad \text{(gas phase)} \tag{12}$$

$$-\nabla\cdot(\frac{\rho_l}{M_l}u_l)+R_w=0 \quad \text{(liquid phase)} \tag{13}$$

Where $D_{o_2}^{eff}$ and D_{v}^{eff} represent the effective diffusivity of the oxygen and water vapor, ρ_l and M_l denote the density and molar weight of the water, R_w is the interfacial transfer rate of water, u_l is the superficial velocity vector based on the total cross-sectional area of fluids and porous medium, which can be obtained from Darcy's law:

$$u_l=-\frac{Kk_{rl}}{\mu_l}\nabla p_l \tag{14}$$

The flow rate of the gas u_g can be derived from Darcy's law:

$$u_g=-\frac{Kk_{rg}}{\mu_g}\nabla p_g \tag{15}$$

2.4. Electrochemical kinetics

Two different potential fields should be considered: one is the potential of the membrane phase, $\emptyset_m$ which governs the transport of the protons, and the other is the potential of the electric phase, $\emptyset_s$ which governs the transport of the electrons. There is no electrochemical reaction in the diffusion layer, and the source term of the electron current is set to zero, the expression is as follows:

$$-\nabla(-\sigma_s\nabla\phi_s)=0 \tag{16}$$

The equation of conservation of electrons and protons in the ACL is described as:

$$\nabla\cdot(-\sigma_s\nabla\phi_s)=-j_a s_a \tag{17}$$

$$\nabla\cdot(-\sigma_m\nabla\phi_m)=j_a s_a \tag{18}$$

Where σ_s and σ_m denote the electric conductivity and the protonic conductivity, respectively. s_a represents the specific surface area of the ACL, j_a represents the anode reaction rate and can be expressed by empirical formula:

$$j_a=i_{Meoh}^{ref}\frac{C_{Meoh}}{C_{Meoh}^{ref}}\exp\left(\frac{\alpha_a F}{RT}\eta_a\right) \tag{19}$$

Similarly, under the influence of methanol permeation, the equation of conservation of electrons and protons in the cathode catalyst layer is described as:

$$\nabla\cdot(-\sigma_s\nabla\phi_s)=j_c s_c-\frac{I_p}{l_{ccl}} \tag{20}$$

$$\nabla\cdot(-\sigma_m\nabla\phi_m)=-j_c s_c+\frac{I_p}{l_{ccl}} \tag{21}$$

$$j_c=i_{O_2}^{ref}\frac{C_{O_2}}{C_{O_2}^{ref}}\exp\left(-\frac{\alpha_c F}{RT}\eta_c\right) \tag{22}$$

Where i_{MeOH}^{ref}, $i_{o_2}^{ref}$, C_{MeOH}, C_{o_2}, C_{MeOH}^{ref}, $C_{o_2}^{ref}$ represent the methanol reference exchange current density, oxygen reference exchange current density, methanol concentration in the ACL, oxygen concentration in the CCL, methanol reference concentration and oxygen reference concentration, respectively.

2.5. Heat transfer

Heat transfer is crucial for a DMFC, the heat transfer of the DMFC:

$$\rho c_p u \cdot \nabla T = \nabla \cdot (k_{eq} \nabla T) + Q \tag{23}$$

The heat transfer of the DMFC system needs to be optimized to overcome the problems such as methanol crossover, water crossover and diffusion of carbon dioxide. In the anode, the heat generated by the electrochemical reactions in the ACL is given by:

$$q_{acl} = i(\eta_a - \frac{\Delta H_a - \Delta G_a}{nF}) \tag{24}$$

Where the first term represents the heat generated by the activation and mass transfer over potentials on the anode, and the second term represents the entropy change of the anodic electrochemical reaction, ΔH_a denoting the anodic reaction enthalpy and ΔG_a represents the Gibbs free energy. Ignoring the joule heat of the membrane, we can use the temperature gradient across the membrane to represent heat q_{acl}:

$$q_{acl} = -\lambda_{men} \frac{dT}{dx} \tag{25}$$

Where λ_{men} represents the effective thermal conductivity of the membrane.

The heat generated in the CCL can be determined by:

$$q_{ccl} = (i + i_p)\eta_c - i\frac{\Delta H_c - \Delta G_c}{nF} - h_v N_{H_2O} \tag{26}$$

Where the first term represents the heat generated by the activation and mass transfer over potentials at the cathode and the mixed potential caused by the methanol crossover through the cathode. ΔH_c denoting the cathode reaction enthalpy and ΔG_c represents the Gibbs free energy. The third term indicates that the liquid water in the CCL evaporates heat. The above formula can also be written as:

$$q_{acl} = (i + i_p)\eta_c - \beta_3 - \beta_4(T_{ccl} - 298) - h_v N_{H_2O} \tag{27}$$

With

$$\beta_3 = \frac{i}{2F}(\Delta H_c^0 - \Delta G_c^0) \qquad \beta_4 = \frac{i}{2F}(C_{H_2O} - \frac{1}{2}C_{O_2})$$

2.6. Cell performance

In the catalyst, the temperature, the anode, the cathode over potentials and the reactant concentrations of methanol and oxygen are determined from the model equations presented above. The cell voltage can be estimated as follows:

$$V_{cell} = E_{cell} - \eta_a - \eta_c - IR_{cell} \tag{28}$$

Where E_{cell} is the thermodynamic equilibrium potentials of the cell. This variable can be determined by:

$$E_{cell} = E_{cell}^0 + \Delta T(\frac{\partial E}{\partial T}) \tag{29}$$

Where the open circuit voltage at 298 K is E_{cell}^0. *I* is the mean current density of the cell, which can be calculated by:

$$I = \frac{1}{l}\int idy \tag{30}$$

R_{cell} is the cell resistance, which is given by:

$$R_{cell} = \frac{\delta_{mem}}{\sigma_m} + R_{contact} \tag{31}$$

Where the first term represents the membrane resistance, with δ_{mem} denoting the membrane thickness, and the second term $R_{contact}$ denoting the contact resistance of the cell.

2.7 Boundary conditions

At the entrance of each flow path, all variables are given based on the reaction condition environment. The boundary conditions at the outlet of each flow path are based on certain assumptions. The assumption is that the laminar flow fully fills the flow path and the concentration gradient of each substance is zero, which the solution is filled with the flow path and the solution is everywhere. Each substance has a uniform concentration distribution. For the external wall, the set flow path is a non-slip flow boundary condition, and the material in the battery including mass transfer is designated as a non-permeable wall surface. The setting of the internal interface conditions of the self-breathing DMFC follows the continuity and material flux balance theory and requires that each internal boundary meet the conditions of the material transfer and material conservation of the entire fuel cell. The detailed boundary conditions are follows.

In the anode, through the external auxiliary equipment such as pump, supplying methanol solution from the feed port to the cell to provide fuel, the boundary speed of methanol solution in the flow inlet, set the inlet is U_m:

$$n * u = U_m \tag{32}$$

The flow channel wall is assumed to be a non-sliding laminar flow, the wall flow rate u_l is set to zero:

$$u_l = 0 \tag{33}$$

The outlet of the flow channel does not have any other force, so the boundary condition of the outlet is set to atmospheric pressure:

$$P = P_{atm} \tag{34}$$

At the entrance of the channel, the concentration of methanol solution supplied to the inlet of the anode flow channel is $C_{m,in}$, which is derived from the material conservation equation, and the liquid saturation is set to 0.95, the boundary conditions for the inlet of the runner are:

$$C_m = C_{m,\text{in}} \qquad S = 0.95 \tag{35}$$

At the interface in the ADL and the ACL, the boundary conditions of the methanol flux is:

$$N_m = \frac{i}{6F} + N_{m,cross} \tag{36}$$

The boundary conditions for the fluid velocities of the ADL and the ACL are:

$$n \cdot u_m = \frac{N_m \cdot M_m}{\rho_l} \tag{37}$$

The boundary conditions of the PEM and ACL are set as follows:

$$n \cdot (\rho_{l,a} u_{l,a}) = N_{Meoh}^{cross} + N_{H_2O}^{cross} \qquad n \cdot (\rho_{g,a} u_{g,a}) = 0 \tag{38}$$

$$n \cdot (-\sigma_m \nabla \phi_m)^{acl} = n(-\sigma_m \nabla \phi_m)^{mem} \qquad n \cdot (-\sigma_m \nabla \phi_s) = 0 \tag{39}$$

$$n \cdot (-D_{Meoh}^{eff} \nabla C_{Meoh} u_{l,a}) = N_{Meoh}^{cross} \tag{40}$$

The boundary conditions of the PEM and CCL are set as follows:

$$n \cdot (\rho_{l,c} u_{l,a}) = 0 \qquad n \cdot (\rho_{g,c} u_{g,a}) = 0 \tag{41}$$

$$n \cdot (-\sigma_s \nabla \phi_s) = 0 \tag{42}$$

$$n \cdot (-\sigma_m \nabla \phi_m)^{mem} = n \cdot (-\sigma_m \nabla \phi_m)^{ccl} \tag{43}$$

$$n \cdot N_{O_2} = 0 \qquad n \cdot N_{HO_2} = 0 \tag{44}$$

In the cathode, the inlet pressure is the atmospheric pressure, that is:

$$p_g = p_{atm} \tag{45}$$

In the cathode diffusion layer and the outer atmosphere interface, the mass fraction of oxygen and the mass fraction of water are:

$$w_{O_2} = w_{O_2,in} \qquad w_{H_2O} = w_{H_2O,in} \tag{46}$$

The liquid saturation is set to 0.05 and the interface potential is equivalent to 0.7V:

$$S = 0.05 \qquad \phi_s = 0.7 \tag{47}$$

At the interface between the cathode diffusion layer and the cathode catalyst layer, the water flux can be described as:

$$N_{H_2O} = \frac{i_c}{2F} + n_d \frac{i_c}{F} \tag{48}$$

The boundary conditions for oxygen flux are expressed as:

$$N_{O_2} = -\frac{i_c}{4F} \tag{49}$$

All the walls of the cell, the boundary conditions are set to insulation or symmetry.

2.8. Model parameters

The setting of the important parameters in the process of establishing the model is shown in Table1:

Table 1. Self-breathing model parameter setting

Parameter	Value	Refs.
Cell length, D	0.008[m]	Assumed
Channel height, H	0.0005[m]	Assumed
Membrane electrode width	0.002[m]	Assumed
Pore radius	0.0004[m]	Assumed
Temperature, T	298[K]	Assumed
Pressure, p-atm	1.013e5[Pa]	—
Gas constant, R	8.314[J/mol·K]	—
Faraday constant, F	96485[C/mol]	—
Molar mass of water, M_{H_2O}	0.018[kg/mol]	—
Molar mass of methanol, M_{MeOH}	0.032[kg/mol]	—
Liquid water density, ρ_{H_2O}	1000[kg/mol]	—
Methanol density, ρ_m	791.7[kg/mol]	—
Water permeability coefficient, $n_d^{H_2O}$	2.9exp(1029×(1/333-1/T))	[28]
Liquid kinetic viscosity, μ_l	0.9×10^{-3}[kg/m/s]	[29]
Gas kinetic viscosity, μ_g	14.96×10^{-6}[kg/m/s]	[29]
Methanol diffusion coefficient, D_m	2.8×10^{-9}exp(2436×(1/333-1/T)) [m^2/s]	[30]
Effective diffusion coefficient of methanol in PEM, $D_m^{eff,pem}$	4.9×10^{-10}exp(2436×(1/333−1/T)) [m^2/s]	[30]
Diffusion coefficient of oxygen, D_{O_2}	$1.775\times10^{-5}\times(T/273)^{1.823}$[$m^2$/s]	[31]
Diffusion layer permeability, K^{ad}	1.2×10^{-12}[m^2]	—
Diffusion layer porosity, ε^{ad}	0.6	—
Surface tension coefficient, σ	0.0625[N/m]	[28]

Electronic conductor conductivity, σ_s	4000[S/m]	[34]
Proton conductor conductivity, σ_m	7.3exp(1268×(1/298-1/T)) [S/m]	[28]
Anode reference current density, i_m^{ref}	94.25exp(35570×(1/353-1/T)) [A/m^2]	[32]
Cathode reference current density, $i_{O_2}^{ref}$	0.04222exp(73200/R×(1/353-1/T)) [A/m^2]	[33]
Reference methanol concentration, C_m^{ref}	1000[mol/m^3]	—
Reference oxygen concentration, $C_{O_2}^{ref}$	0.21*p_atm/(R*T) [mol/m^3]	—
ACL transfer coefficient, α_a	0.35	[28]
CCL transfer coefficient, α_c	0.8	[28]
Methanol oxidation reaction equilibrium potential, E_a^{eq}	0.046[V]	[29]
Oxygen reduction reaction equilibrium potential, E_c^{eq}	1.223[V]	[29]
Enthalpy of anode reaction, Ha	130.98e3[J/mol]	—
Anode Gibbs free energy, Ga	9.35e3[J/mol]	—
Enthalpy of the cathode reaction, Hc	-857.49e3[J/mol]	—
Cathode Gibbs free energy, Gc	-711.24e3[J/mol]	—
Oxygen supply concentration, $C_{O_2}^{feed}$	8.58[mol/m^3]	—
Contact resistance, $R_{contact}$	8×10^{-5}[Ωm^2]	[34]

The self-breathing three-dimensional two-phase model established in this paper couples multiple physical fields, including material conservation, material transport, momentum transport, proton and electron transport and heat transfer. The entire model consists of four computational regions, divided into 520,000 degrees of freedom and meshed volumetric maps as shown in 1 below. Make the calculation process as accurate as possible.

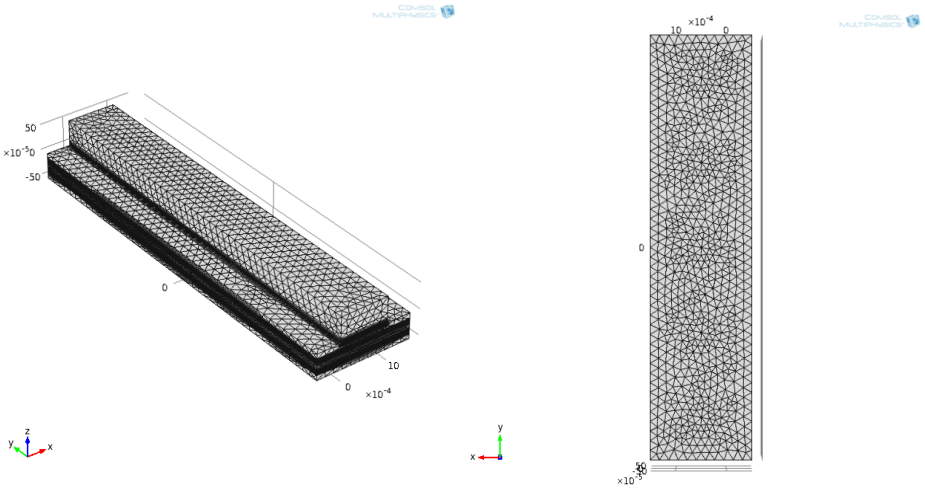

Figure 2. The mesh of the model

3. RESULT AND DISCUSSION

3.1. Effect of reactant concentration

In order to study the effect of methanol concentration on the performance of self-breathing DMFC, the model was simulated and analyzed when the methanol concentration was 0.5M, 1.0M, 1.5M and 2.0M, respectively. Fig.3 (a) shows the distribution of the methanol concentration at 1.5M. It can be seen from the figure that the methanol concentration in the flow channel is high and constant. This is because the transmission of methanol in the flow channel mainly relies on convective movement. Under the certain flow velocity, the consumed methanol will be supplied rapidly. The concentration of methanol in the diffusion layer is lower and varied obviously, because the process of methanol transmission from the anode channel to the diffusion layer is hindered by the current collector and the anode porous medium, it mainly depends on the diffusion movement [27]. Fig.3 (b) shows the distribution of the methanol concentration in the anode diffusion layer at 1.5M. It can be observed that the methanol concentration decreases in the direction of methanol flow. The trends of the distribution of the methanol concentration predicted by the model presented in this paper are in accordance to the ones proposed by W.W. Yang [27, 28].

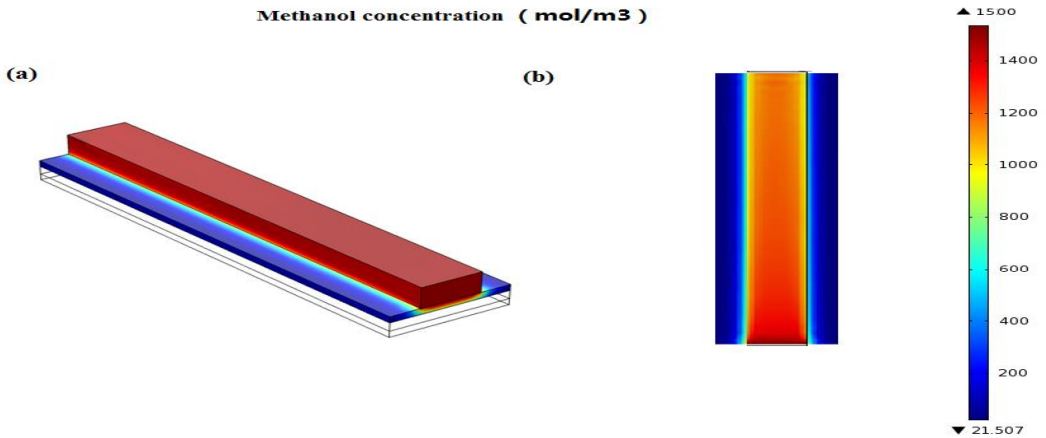

Figure 3. (a) Distribution of the methanol concentration in the anode channel and diffusion layer. (b) Distribution of the methanol concentration in the anode diffusion layer.

The effect of methanol concentration on cell performance is mainly reflected in two phenomena: the increase in methanol concentration leads to an increase in the coverage of methanol on the catalyst layer, leading to an increase in the concentration gradient of methanol at the anode and cathode and methanol permeation through the nafion membrane. Another important problem is that the polarization characteristics of the mass transfer region are directly related to the methanol concentration, while increasing the current density means an increase in the limit current density. Fig.4 shows the power density and the UI curve of the cell. The simulation results show that when the methanol concentration is low, the open circuit voltage is higher [29]. When the voltage fluctuates between 0.4v and 0.7v, the current density of the ACL is maximized when the concentration of the methanol solution is 0.5M. When the voltage is smaller under the simulation parameters, the difference in current density between different concentrations of methanol solution is greater. At the same time, the higher the concentration of the methanol solution, the greater the current density. It can be concluded that the performance of the cell is better when the methanol concentration is 1.5M. As reported in previous works [29-33], the optimum methanol concentration range is 1M to 2M. So our conclusion is reasonable.

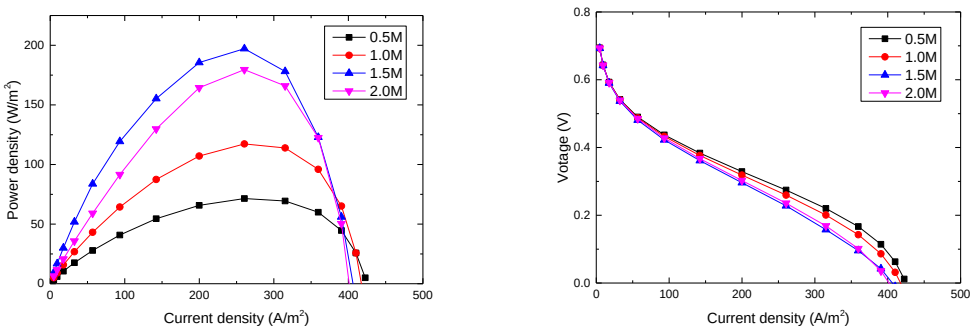

(a) (b)

Figure 4. Model predictions for power density (a) and voltage (b) with varying current density for different

Fig.5 shows the distribution of oxygen concentration in the cathode. It can be seen from the figure that the oxygen concentration is the largest in the vent hole and decreases from the inlet center to the periphery. The diffusion coefficient of the gas is large, so the distribution of oxygen concentration in the cathode porous medium is not as obvious as the methanol concentration distribution, and the concentration change range from the CDL to the CCL is very small (The minimum oxygen concentration is 7.1341 and the maximum value is 7.35). The distribution of oxygen affects the reaction rate of the catalytic layer. The higher the oxygen concentration, the higher the reaction efficiency. V.B. Oliveira [34] also analyzed the oxygen distribution of the cathode, but he did not adequately consider the effect of the vent hole on the gas distribution. Compared to his results, our data is more comprehensive and closer to the actual situation.

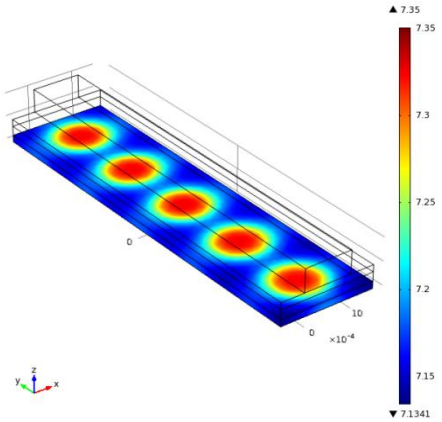

Figure 5. The distribution of oxygen concentration in the cathode

3.2. Effect of flow velocity and the pressure

Fig.6 is the volume distribution of liquid pressure in anode porous media. The liquid pressure is greatest at the liquid inlet and decreases along both sides of the inlet. The methanol solution moves in the direction of decreasing pressure. The movement speed of methanol is set in the y direction. Therefore, with the obvious convection in the y direction and the existence of convection in the methanol solution, the corresponding current is collected. Sublayer methanol transports faster. Since the pressure of the cathode liquid is higher than that of the anode, convection is caused, which significantly hinders the transport of the liquid and the transfer of methanol is mainly diffusion, so the pressure in the z direction does not change significantly. In the anode range, the pressure distribution of the liquid phase mass will have a certain degree of influence on the movement of the mass. For example, if the pressure difference of the methanol solution is high, the convection is obvious. It can be seen from the figure that the anode liquid pressure is almost constant, and it is similar to atmospheric pressure. The reason for this phenomenon is that the methanol solution is distributed throughout the porous medium and that the rate of methanol in the anode reaction is not significant and the convection is not severe. It is confirmed that the transfer process of methanol is largely through diffusion. The result is consistent with the conclusion obtained by Dingding Ye [36].

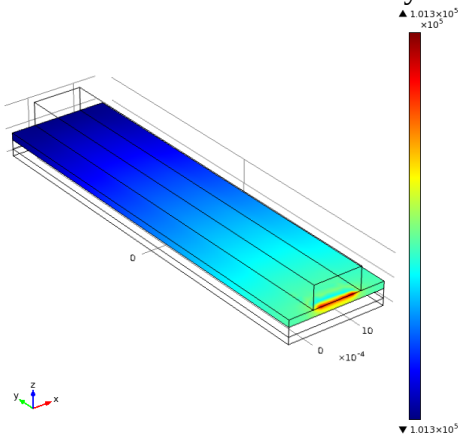

Figure 6. Volume distribution of liquid pressure in anode porous media

Fig.7 is the gas pressure distribution in the cathode porous media. It can be seen from the figure that the oxygen pressure at the inlet is the largest and the pressure is gradually reduced with the inlet as the center. The variety of gas pressure in the cathode porous media is very small, because a large amount of material in the cathode porous medium is gas and the gas flow properties are very good. When the cathode oxygen pressure is large, there are many advantages that can hinder methanol permeation, weaken the polarization phenomenon and improve the cathode reaction. Another key point is that increasing the pressure can promote the water to reach the proton exchange membrane faster and better, thereby increasing the water content of the proton exchange membrane and reducing the internal resistance of the proton exchange membrane, thereby enhancing the cell performance.

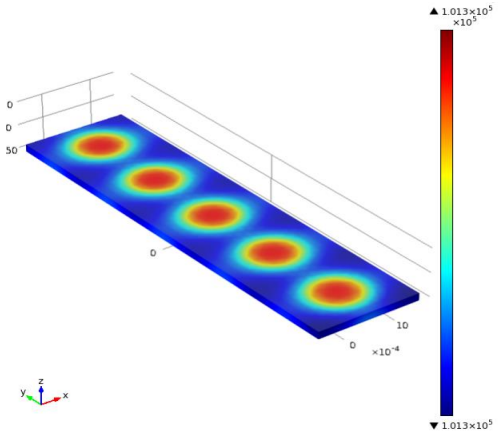

Figure 7. Distribution of gas pressure in cathode porous media

When the concentration of methanol solution is 1.5M, the anode flow velocity distribution is shown in Fig.8 and the flow rate is indicated by arrows in the vector diagram. If the size and direction of the arrow has a certain directionality, it can indicate the speed and direction of the flow, respectively. The flow velocity in the porous media corresponding to the flow channel is more balanced and the flow velocity at the edge of the runner and the ridge is greater. Due to the methanol permeation, if the flow velocity of the methanol solution is too fast, the hydraulic pressure becomes large, and the mixing potential generated by the penetration is greater, which lowers the cell performance; but if the methanol flow velocity is too slow, the cell performance is not high.

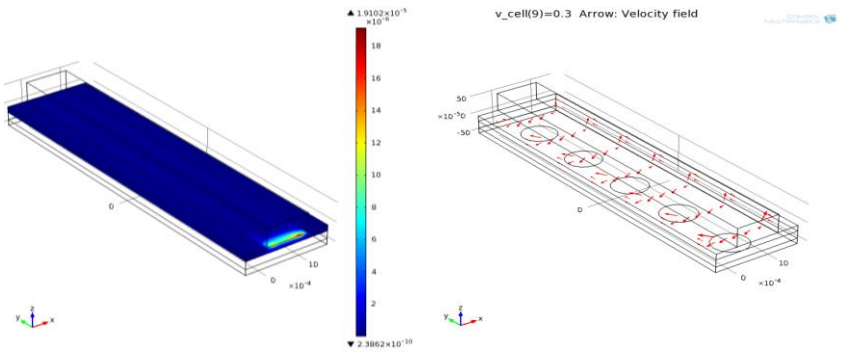

Figure 8. Distribution of flow velocity in the anode

The effect of different methanol flow velocity on the cell performance is shown in Fig.9. These curves are obtained at a methanol concentration of 1.5M. The flow velocity of the methanol solution were 0.0009m/s, 0.0016m/s, 0.0023m/s, 0.003m/s, respectively. When the methanol flow rate is increased from 0.0009m/s to 0.003m/s, the voltage can be obtained within the range of low current and the voltage is almost the same. However, when the current density increases again, the difference in cell performance is apparent depending on the rate of supply. When the mass is transported, if the flow velocity is too small, the limited is still very obvious. The reason is that the generated bubbles cannot be effectively discharged to the outside during the whole operation, if the current density is small. Therefore, the bubble block will occupy a certain area, which is not conducive to mass transfer. It can be seen from the figure that not the greater the flow rate, the cell performance will be better. We can think that this situation is caused due to methanol penetration. We can also clearly know from the figure that there is a state of equilibrium in the case where the mass transfer is restricted and the methanol is permeable to the cathode. The result of this model is that when the methanol concentration is 1.5M, it is reasonable to synthesize other factors to take the flow rate at 0.0016m/s. When the concentration of methanol solution is 1.5M, the oxygen flow velocity distribution is shown in Fig 10. As can be seen from the figure that the gas flow velocity at the edge of the pores is higher while the flow velocity at the center of the pore is lower. All the pores are the channels of the gas mixture. In the self-breathing geometry designed by this model, the pores not only serve as the inlet for reactant O_2 but also form the outlet for the production of product H_2O. Oxygen is continuously consumed because of the oxidation reaction, after transported by the pores to the porous medium. At the same time, the water vapor is generated and the water is removed through the cathode porous medium, during the reaction process.

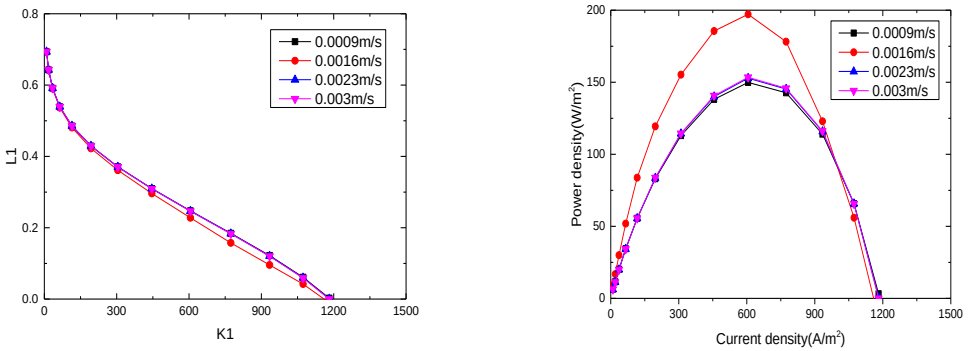

(a) (b)

Figure 9. Variation of power density (a) and voltage (b) with current density at different methanol flow rates

It can be seen from the mutual restriction between the products and the consumables that the volume of the gas constituted by each component will increase. Therefore, the mixed gas in the cathode porous medium flows outwards for the purpose of continuous reaction. The figure shows that the maximum velocity appears at the edge of the hole. This is because the resultant (water vapor) accumulates in the active layer under the current collector and is discharged directly from the edge of the hole. In contrast, the gas flow rate at the center of the hole is relatively small, because the product

of the pore area is discharged directly from the area.

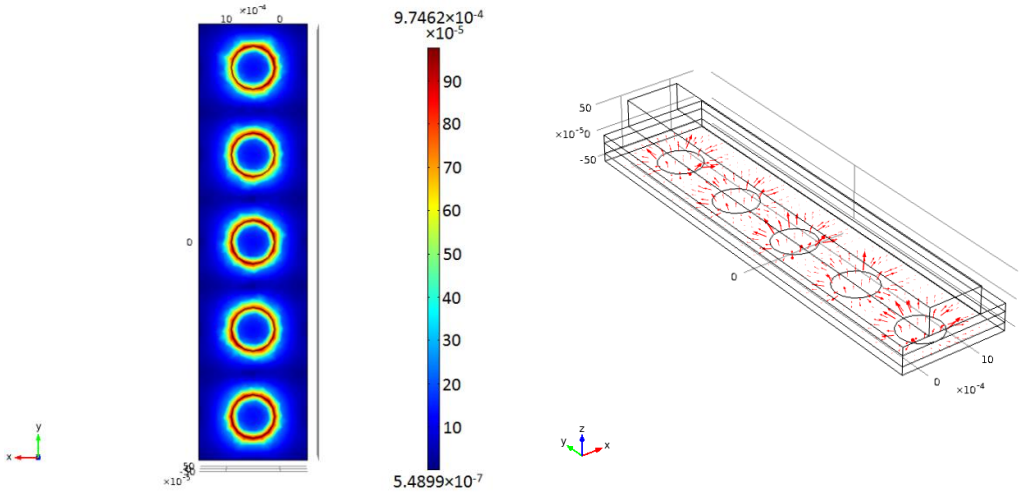

Figure 10. Distribution of oxygen flow rate

3.3. Distribution of liquid saturation

In order to simplify the mathematical model, the catalytic layer is simplified as a plane. The distribution of liquid saturation in the porous anodic medium is shown in figure 11. The saturation of the diffusion layer corresponding to the flow channel is higher, and the saturation is smaller in the sub-ridge. In the z-direction, the liquid saturation decreases along the ADL to the ACL. The reason for this phenomenon is that the amount of methanol solution is reduced due to the anodic reaction, carbon dioxide is generated, resulting in an increase in gas content, and a confluence of methanol solution and carbon dioxide convection.

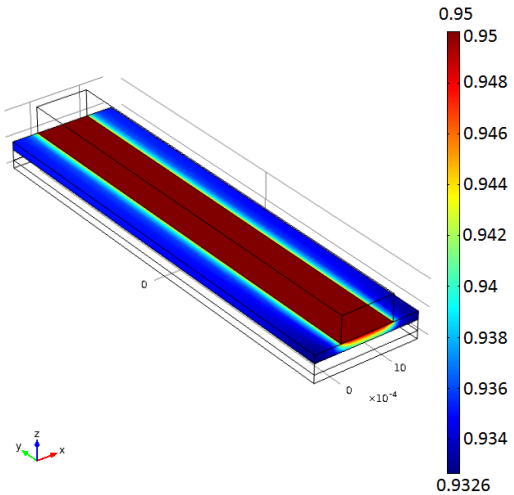

Figure 11. Distribution of liquid saturation in the anode

Whether the water produced by cathode reduction reaction can be quickly removed is the main factor determining the output performance and stability of the cell. Fig.12 shows the liquid saturation distribution of the cathode diffusion layer. It can be seen from the figure that the saturation increases

with the diffusion zone around the gas port, and the fuel inlet presents an increasing trend towards the outlet.

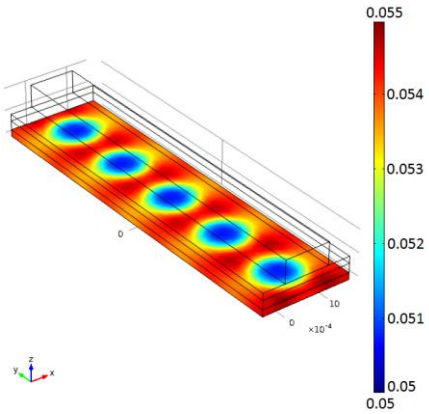

Figure 12. Distribution of liquid saturation in the cathode

Air-breathing μDMFC has no auxiliary oxygen supply device, the cell structure is relatively simple, but there is a disadvantage that the cell is not conducive to water transmission. When the cell is in operation, the water generated by the reaction needs to be transferred to the outside of the cell through the CDL. Because it is air-breathing, oxygen flow rate will not be high, which cause the water cannot be timely and effectively out of the cell, causing "flooding". "Flooding" is the key factor to limit discharge performance. The water vapor generated by part of the electrochemical reaction is converted into a liquid. The water left in the CDL is not conducive to gas transmission to a certain extent, and the effective reaction area is reduced in disguise, which is detrimental to the performance of the cell. But the operation of the cell must have the participation of water that is the product. However, the PEM as the electrolyte layer must have a strong proton conductivity, a very weak electron conductivity and chemical properties cannot be active, so it must contain a solid polymer membrane and liquid water, so that protons can be transmitted normally and efficiently. Therefore, maintaining a good balance of balance is quite critical and is a guarantee of cell performance.

3.4. Distribution of potential and current density

Fig.13 is the distribution of proton current density. In the proton exchange membrane region corresponding to the flow channel, the proton flow has a high density and decreases toward both sides. In the Z direction, the cathode catalyst layer slowly decreases. The distribution of proton flow and the magnitude of the value reflect the reaction of the anode to a certain extent. The proton are generated in the ACL and transported in the PEM, reacts with oxygen and electrons to generate water the CCL. Fig. 14 shows the distribution of the electron current density in porous media.

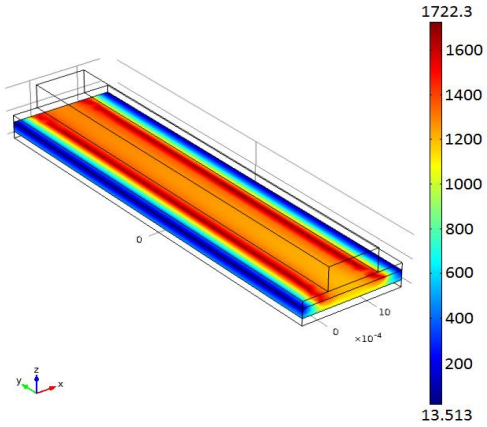

Figure 13. Distribution of proton current density

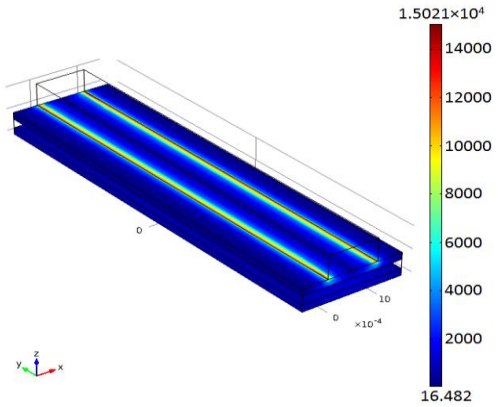

Figure 14. Distribution of the electron current density

It can be seen from the figure that the distribution of the electron current density changes with the shape of the current collecting layer, the electron current reaches the peak at the edge of the current collecting layer on both sides of the flow channel.

The current density distribution of the ACL is shown in Fig.15. It can be seen from the figure that the current of the ACL decreases from the middle to both sides in the xy plane, and the current density distribution of the ACL depends on how the methanol is distribution. The concentration of methanol in the corresponding catalytic layer under the channel is higher, and the current density in the catalytic layer corresponding to the flow channel is higher and the change is weak. Due to the drastic decrease of the concentration of methanol in the diffusion layer, the corresponding current density under the ridge is drastically reduced. The higher the effective diffusion coefficient of methanol, the more able to promote the transmission of methanol to the anode catalytic layer. The higher the catalytic activity of the catalyst layer, the more efficient oxidation of methanol. It will have a higher electronic conductivity, more convenient for electronic transmission. Larger methanol concentrations and over voltages produce local current densities that result in uneven distribution of anode current density. The overall trend of current density is the same as the conclusion of R. Chen [26] and W.W. Yang [28], but compared to their data, our data on the variation in current density of the flow channel is more detailed and comprehensive.

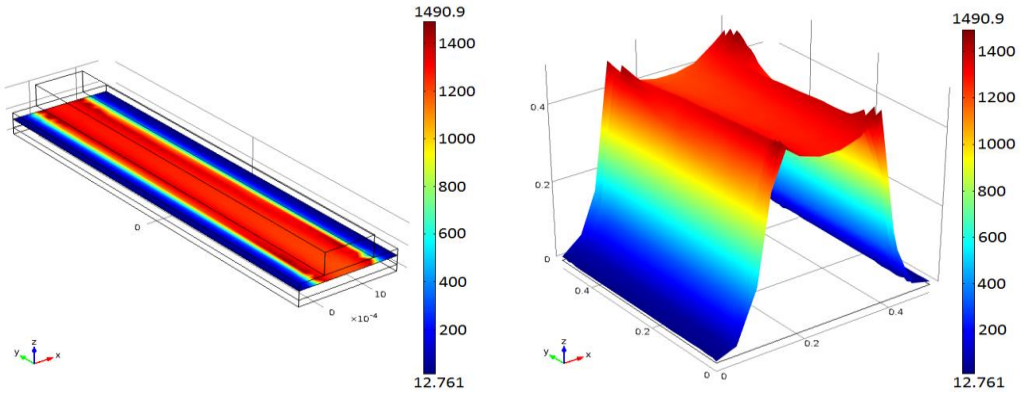

(a) (b)

Figure 15. The current density distribution of the ACL

It can be seen from Fig.16 that the current density distribution of the CCL is similar to that of the anode catalytic layer, and it decreases from the corresponding position of the flow channel to both sides in the XY plane. The cathode reduction reaction requires the participation of oxygen and the proton electrons generated by the anode oxidation reaction, so the reaction of the CCL depends on the reaction of the anode and the oxygen concentration. From the above analysis of the anode reaction, it can be seen that the concentration of the methanol solution in the flow channel is higher, the current density of the CCL corresponding to the flow channel is higher. In the range of the ridge, the product distribution of the anode is less, and the oxygen concentration is slightly lower, the corresponding cathode current density is smaller.

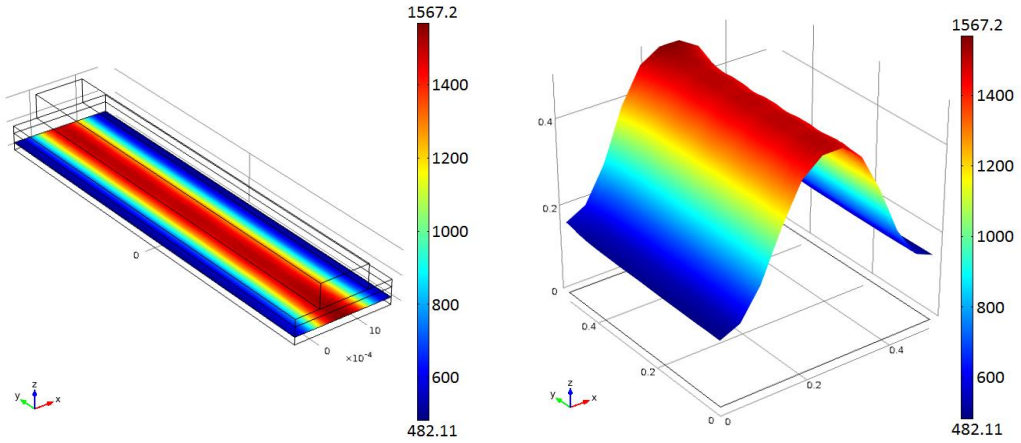

(a) (b)

Figure 16. The current density distribution of the CCL

3.5. Effect of temperature

As can be seen from fig.17 and fig.18, the overall temperature distribution of the μDMFC is reduced from the inlet to the outlet of the raw mass and is the lowest at the point where the product is excluded. In the Z direction, the temperature increases from the anode channel to the cathode, and the temperature is highest at the CCL. The mass transfer and water management in μDMFC will have a

restricted effect on the temperature distribution inside the cell, such as when water is discharged, it will take away part of the heat. Conversely, the temperature also affects mass transfer, water management and catalyst activity, so the temperature is very important to the operation of the cell. Appropriate to enhance the temperature, the cell performance also increased. The performance of the cell is good at higher temperature, mainly because the electrochemical activity of the catalyst is directly proportional to the temperature, and the reaction rate is improved. Moreover, with the increase of temperature, contribute to the transfer of mass. The increase of temperature will also result in the increase of oxygen diffusion rate, and promote better transmission. At the higher temperature, the water evaporation rate of the cathode increases, which slows down the water flooding. The PEM in the higher temperature environment, the ionic resistivity becomes smaller, conduction capacity and velocity are accelerated. However, too high temperature will lead to serious methanol penetration. The temperature is still compatible with other parameters such as reactant concentration, flow rate, pressure and so on, there will be a better performance of the cell equipment.

When the methanol concentration is 0.5M, 1M, 1.5M, 2M, the temperature distribution of the open circuit is shown in fig.18. As can be seen from the figure, the temperature distribution and the amount of the change in the cell varies with the concentration of the feed. In the extreme case of open circuit, most of the heat is generated by the reaction of the penetration of methanol and oxygen which is consumed in the catalytic layer. Methanol permeability will change according to the concentration of methanol, the rule is that the concentration is more concentrated, the effect is more intense. Accordingly, the temperature of the fuel cell is increased at a high concentration of the feed material. The increase of temperature leads to strong natural convection in the channel, so the whole cell system has obvious temperature difference.

The result is similar to the results obtained by V.B. Oliveira [34] and R. Chen [26]. But our results are more comprehensive because we can get the temperature distribution of each part of the cell.

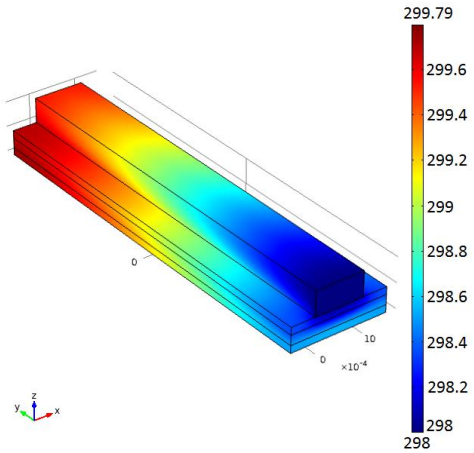

Figure 17. Volume distribution of cell temperature

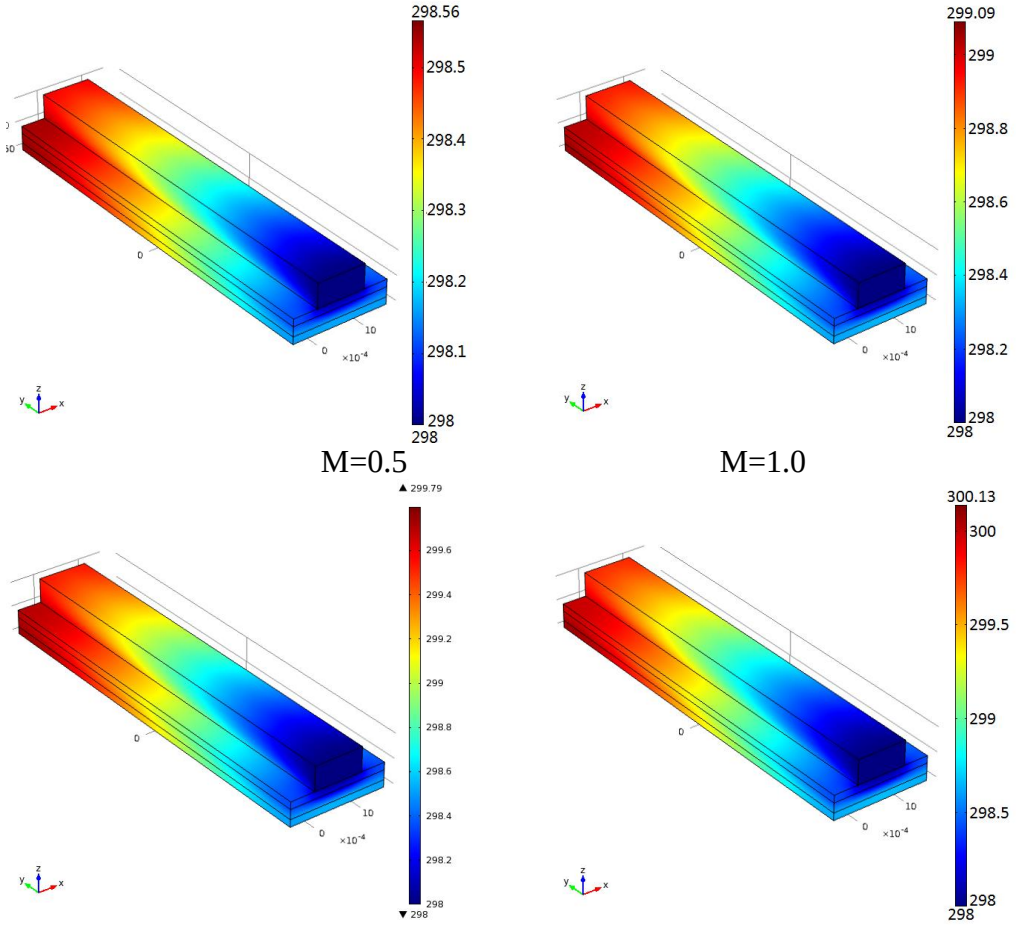

Figure 18. Volume distribution of cell temperature under different methanol concentration

4. CONCLUSIONS

This paper developed a three-dimensional two-phase non-adiabatic model for air-breathing micro DMFC, the computational domain includes: flow channels, porous media, and PEM. Mainly to improve the cathode structure, thus enhancing the performance of DMFC under the condition of the air-breathing. The components of the model and the influence of the distribution on the performance of the cell was analyzed. Based on the simulation results, the following conclusions are obtained:

1) The feeding condition of the cell has a great influence on the results. The fuel concentration decreases along the channel to the PEM. The oxygen concentration is reduced from the diffusion layer to the catalytic layer, but the concentration difference is less than the concentration difference of methanol in the cathode. Within a certain range, increasing the concentration of methanol is beneficial to achieve better performance. Increasing the oxygen concentration in the cathode can also significantly increase the performance.

2) When the cell is initially operated to discharge to an external load, the voltage drops sharply and then slowly. When the current density is constant, the phenomenon of methanol permeability is related to the fuel. The performance of this phenomenon can be intensified when the concentration is high. The increase in the operating temperature can also increase methanol penetration.

When the cathode hydraulic pressure is greater than that in the gas, the flow of liquid to the anode can be promoted, and the penetration phenomenon can be effectively inhibited.

3) The proton potential is mainly affected by the concentration of methanol. If the methanol concentration distribution is not uniform, it can lead to the non-uniform distribution of proton potential. The electron flux density is mainly affected by the shape of the current collecting layer.

4) In the anode flow field, the liquid saturation decreases with the movement trend, and the porous media module slowly decreases along the direction of motion. The saturation of the liquid phase of the cathode changes slightly along the direction of methanol movement. As the reaction proceeds, the content of the liquid phase substance in the anode porous medium increases, resulting in obstruction of the gas movement and leading to significant differences in pressure.

ACKNOWLEDGEMENTS

This work is supported by the National Natural Science Foundation of China (Grant no. 61704041), the National Natural Science Foundation of china (Grant no.61411136003) and the Key research and development projects of Zhejiang Province (Grant no.2017C01056).

References

1. Y. Jiang, X. Wang, L. Zhong, L. Liu, *J. Micromech. Microeng*, 16 (2006) S233.
2. B. Zhang, Y. Zhang, H. He, J. Li, Z. Yuan, *J. Power Sources*, 195 (2010) 7338-7348.
3. Y.F. Zhang, L.W. Wang, Z.Y. Yuan, S.B. Wang, J.M. Li, *Sci Bull*, 56 (2011) 826-829.
4. H. Yang, T.S. Zhao and Q. Ye, *J. Power Sources*, 139 (2005) 79-90.
5. J. Parbhuram, T.S. Zhao, C.W. Wong, J.W. Guo, *J. Power Sources*, 134 (2004) 1-6.
6. V. Saarinen, O. Himanen, T. Kallio, G. Sundholm, K. Kontturi, *J. Power Sources*, 172 (2007) 805-815.
7. R. Chen, T.S. Zhao, J.G. Liu, *J. Power Sources*, 157 (2006) 351-357.
8. J.G. Liu, T.S. Zhao, Z.X. Liang, R. Chen, *J. Power Sources*, 153 (2006) 61-67.
9. N. Sabate, J.P. Esquivel, J. Santander, N. Torres, I. Gracia, *Microsyst Technol*, 14 (2008) 535-541.
10. R. Chen, T.S. Zhao, *J. Power Sources*, 167 (2007) 455-460.
11. T.S. Zhao, R. Chen, W.W. Yang, C. Xu, *J. Power Sources*, 191 (2009) 185-202.
12. A. A. Kulikovsky, *Electrochem. Commun*, 6 (2004) 1259-1265.
13. P. Argyropoulos, K. Scott, A.K. Shukla, C. Jackson, *J. Power Sources*, 123 (2003) 190-199.
14. R. Chen, T.S. Zhao, *J. Power Sources*, 152 (2005) 122-130.
15. K.T. Jeng, C.W. Chen, *J. Power Sources*, 112 (2002) 367-375.
16. K. Scott, W. Taama, J. Cruickshank, *J. Power Sources*, 65 (1997) 159-171.
17. J. Prabhuram, T.S. Zhao, Z.X. Liang, R. Chen, *Electrochim. Acta*, 52 (2007) 2649-2656
18. D.S. Falcão, J.P. Pereira, C.M. Rangel, A.M.F.R. Pinto, *Int. J. Hydrogen Energy*, 40 (2015) 5408-5415.
19. H. Bahrami, A. Faghri, *J. Power Source*, 230 (2013) 303-320.
20. J.P. Meyers, J. Newman, *J. Electrochem. Soc*, 149 (2002) A718-A728.
21. Q. Ye, T.S. Zhao, C. Xu, *Electrochim. Acta* 51 (2006) 5420-5429.
22. G. Murgia, L. Pisani, A.K. Shukla, K. Scott, *J. Electrochem. Soc*, 150 (2003) A1231-A1245.
23. A. A. Kulikovsky, *Electrochem. Commun*, 7 (2005) 237-243.
24. L. Wang, Y. Zhang, Z. An, S. Huang, Z. Zhou, *Energy*, 58 (2013) 283-295.
25. W. W. Yang, T. S. Zhao and C. Xu, *Electrochim. Acta*, 53 (2008) 853-862.
26. R. Chen, T.S. Zhao, W.W. Yang, C. Xu, *J. Power Sources*, 175 (2008) 276-287.

27. W. W. Yang, T. S. Zhao and C. Xu, *Electrochim. Acta*, 53 (2008) 853-862.
28. W. W. Yang, T. S. Zhao, *J. Power Sources*, 174 (2007) 136-147.
29. Y.C Park, D.H. Kim, S. Lim, S.K. Kim, D.H. Peck, *Int. J. Hydrogen Energy*, 37 (2012) 4717-4727.
30. B. Zhang, Y. Zhang, H. He, J. Li, Z. Yuan, *J. Power Sources*, 195 (2010) 7338-7348.
31. Y. Tang, W. Yuan, B. Tang, Z. Li and M. Pan, *J. Power Sources*, 195 (2010) 5628-5636.
32. T.S. Zhao, C. Xu, R. Chen, W.W. Yang, *Prog. Energy Combust. Sci*, 35 (2009) 275-292.
33. Q. Liao, X. Zhu, X. Zheng, Y. Ding, *J. Power Sources*, 171 (2007) 644-651.
34. V. B. Oliveira, C. M. Rangel and A. M. F. R. Pinto, *J. Power Sources*, 196 (2011) 8973-8982.
35. D. Ye, X. Zhu, Q. Liao, J. Liu, Q. Liu, *J. Power Sources*, 192 (2009) 502-514.
36. M. A. R. Biswas, S.P. Mudiraj, W.E. Lear, O.D. Crisalle, *Int. J. Hydrogen Energy*, 39 (2014) 8009-8025.
37. S. Yousefi, M. Zohoor, *Int. J. Hydrogen Energy*, 39 (2014) 5972-5980.
38. N.K. Shrivastava, S. B. Thombre and R. K. Mallick. *Electrochim. Acta*, 149 (2014) 167-175.
39. R. Xue, Y.Zhang, X. Liu, *Energy*, 139 (2017) 535-541.
40. Z. Xiong, S. Liao, D. Dang, X. Tian, S. Hou, *Int. J. Hydrogen Energy*, 40 (2015) 3961-3967.